Heliyon 7 (2021) e06856

Contents lists available at ScienceDirect

Heliyon

journal homepage: www.cell.com/heliyon

Research article

Ballistic performance of Polycarbonate and Polymethyl methacrylate under normal and inclined dynamic impacts

Shabnam Sadeghi Esfahlani *

Anglia Ruskin University, Engineering and the Built Environment, CM1 1SQ, Chelmsford, Essex, United Kingdom

ARTICLE INFO

Keywords:
Polycarbonate (PC)
Polymethyl methacrylate (PMMA)
High Strain Rate Materials
Residual Velocity
Depth of Penetration (DOP)
Path of Penetration (POP)

ABSTRACT

Polymeric materials have exceptional mechanical properties, making them attractive for automotive, aerospace, defence and buildings industries. The numerical analysis of translucent polymeric materials' ballistic performance is investigated to analyse the deflection and perforation performance at high impact velocities. Computational methods are exploited to predict the ballistic performance of thick targets and projectile damage, and the results are validated against published works. The 3D numerical analysis is conducted by simulating plates and projectiles' mechanical performance that controls the deflection and ricochet procedure. Impact damage analysis is undertaken on monolithic Polycarbonate (PC) and Polymethyl methacrylate (PMMA) targets under various impact velocities, projectile's core density with inclined 30° and normal 90° impact angle. The results are analysed in terms of failure performance, depth of penetration (DOP), penetration path (POP), and residual velocity. The numerical analysis is further developed to investigate the projectile's impact velocity effects on the DOP and its direction. The results showed that the DOP changes linearly with the impact velocity, where the POP is as yet nonlinear. Extended Drucker Prager Strength (EDP) material model with the failure criteria of principal stress and tensile pressure failure is used to simulate the brittle-ductile PMMA target's performance under dynamic impact. Shock Hugoniots equation of state with plastic strain failure is conducted to affect PC plates' tensile performance.

1. Introduction

Polymers are fundamental in a variety of engineering applications for their exceptional mechanical properties, specifically, excellent strength to weight ratios [1]. These materials have rate-subordinate mechanical properties, high durability and minimal cost [2]. The ballistic performance of amorphous polymers at high speed has a significant role in designing protective structures, such as military, nuclear reactor vessels, and bulletproof shields. Three critical properties can be assigned to glassy polymers, including high dynamic compressive strength, high brittleness, transparency and low density, which is the quality of amorphous homopolymers [3].

Amorphous polymers' experimental material investigation was conducted by various researchers where it is identified as thermally activated molecular movements processes described by the state transition theory, the conformational change theory, and the intermolecular shear resistance model [4]. The intermolecular shear resistance model depends on a specific range of temperatures and strain rates. There are two phases over a wide range of temperatures and strain rates while describing amorphous polymers' yield behaviour. Transition is associated with a spiked rise in yield stress and polymer chains' secondary relaxation with the precise molecular process. Different trial concentrates likewise have explored the impact of the compressive pressure strain of indistinct polymers under various strain rates and temperature. Varghese and Batra [5] showed that for the PMMA, the α and β transition temperature shifts are more like compared to the PC. The capacity modulus value is higher in the glassy state than in the rubbery state. Mulliken and Boyce [6] have done a uniaxial compression test and proposed constitutive relations to simulate glassy polymer's mechanical deformation. Their examination showed some sub-atomic movement, separate from molecular manners of the α shift, which has an independent commitment to the naturally visible rate dependency of these substances. Richeton et al. [7] presented the compressive experimental study of amorphous polymers under strain rates ranging (10^{-4} s^{-1} to $5e^{3}$ s^{-1}) and temperatures of ($40\,°C$ to $180\,°C$) in that, a modified Split-Hopkinson pressure bar was integrated to test materials under dynamic loading. Mulliken and Boyce [6] illustrated that PC and PMMA display raised yield rate sensitivity following the identical strain rate conditions

* Corresponding author.
E-mail address: shabnam.sadeghi-esfahlani@aru.ac.uk.

https://doi.org/10.1016/j.heliyon.2021.e06856
Received 29 April 2020; Received in revised form 30 December 2020; Accepted 15 April 2021

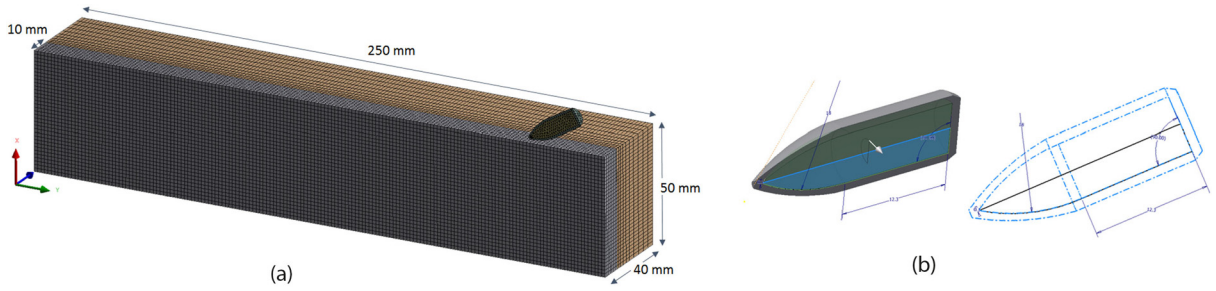

Fig. 1. (a) The half model of the projectile impacting a PMMA plate at an angle of inclination of 30°. (b) 0.3″ bullet.

as the β shift of the viscoelastic behaviour. These experimental studies showed that throughout low to average rate compression examination on the servo-hydraulic apparatus, both PC and PMMA samples deform in a ductile way up to a true strain of 0.80. Satapathy and Bless [8] showed that amorphous polymer material confines during dynamic testing and the confinement delay micro failure mechanisms that cause nucleation in this brittle material and consequently its failure. PMMA dynamic investigation showed that the material's restriction may defer breaking at the advantage of a ductile shear failure mechanism. Rittel and Brill [9] conducted the static and dynamic mechanical review of cylindrical PMMA subject to compression and determined its rate and pressure sensitivity over a diverse range of strain rates. The quasi-static state demonstrated ductility behaviour. The dynamic failure mode contained axial splitting and confining pressure at lower strain rates and adiabatic shear formation of a conical plug at higher strain rates. The ballistic resistance of GFRP laminates subjected to high-velocity impact was studied by Chen et al. [10]. Three elements, including layer angle, stacking sequence and proportion of different layer angles, were considered. An orthogonal test technique was utilized for the investigation, which can lessen the quantity of simulations adequately without sacrificing the result's accuracy. The outcome demonstrated that the laminate with layer angles 0°/90° and ±45° presented greater ballistic resistance than the other angle pairs.

The examination by Zhang et al. [11] explored the ballistic execution of two diverse primary fibre metal laminates exposed to high-speed diagonal effect by impact by rigid hemispherical nose projectile with 0°, 30°, 45° and 60° angles. Their results showed that the projectile diverges during the oblique impact, and the deflection angle diminishes with rising impact velocity. Chen et al. [12] studied the normal and oblique ballistic collision behaviour of glass fibre-reinforced metal laminate impacted by a rigid cylindrical missile with different impact angles. It was shown that standard impact had a higher ballistic limit velocity than that of oblique one while the ballistic limit velocity at 45° is slightly higher than that at 30°.

In this study, three-dimensional constitutive models were simulated to investigate the mechanical performance of PC and PMMA targets subjected to 0.3″ projectile. Ballistic impact of monolithic targets is conducted using numerical simulation under the inclined impact of 30° and normal inclined of 90° to analyse the maximum depth of penetration (DOP) and path of penetration (POP) of the projectile in these amorphous polymers considering various parameters such as; angle of initial velocity, projectile core density, impact velocity. Various experimental analysis performed in literature quantified comparison of target and projectile's damage and penetration is conducted to validate simulated models' accuracy. It is used to investigate the DOP, POP ballistic limit and residual velocity with various projectile core density 7800, and 5850 kg/m^3 and impact velocity $720, 600, 500, 400, 300$ $\frac{m}{s}$. The damage and degree of it are significant measurements that must be replicated in an accurate numerical model of bullet-glass interaction.

2. Numerical analysis

3D FE modelling of the target and projectile were simulated using half symmetry, as shown in Fig. 1(a), (b). The target's dimension is $250 \times 50 \times 40$ (mm^3), and the bullet's radius is 4.8 mm, with an overall length of 35 mm. The target and projectile were meshed using the MultiZone hexahedral method and Automatic method, respectively. A general contact algorithm of ANSYS Workbench is used, and the material's failure controls the erosion.

2.1. Projectile's inclined and normal impact on target

Numerical analysis of the projectile was simulated considering a simple Von-Mises yield criterion in that the deformation and failure of the kinetic projectile are negligible in a penetration process. The projectile motion and its penetration procedure were analysed given being a rigid-body [13]. 4340 Steel and Copper were comprised in that the strain hardening effects were neglected. Two impact angles 30° and 90° were simulated to investigate the DOP and POP at the targets and illustrated in Fig. 2.

2.2. Material model of PMMA and PC

The materials utilized in this examination were two amorphous polymers, Polycarbonate (PC) and Polymethyl methacrylate (PMMA) with the material properties taken from [6]. The overall reaction of the polymers is very similar over the wide scope of temperatures and strain rates, and the reliance on strain rate is negligible [14]. These results are validated with the experimental study presented in [7]. An initial elastic reaction followed by yielding, strain softening, and a sensational strain solidifying result from adiabatic heating. This adiabatic temperature rise is observable through the large deformation of the samples. In the high rate testing, the PC specimens deformed in a ductile manner over the high strain rates, 1200 s^{-1} to 4000 s^{-1} (actual strain rate at yield). The grade of the flowing arch diminishes (diminishing strain hardening rate) with strain rate increments. PMMA's strain hardening totally vanishes at high strain rates because of the adiabatic heating effects, and for PC, the adiabatic heating has much less impact on the strain hardening rate. The flow stress of PMMA is more receptive to temperature than that of PC. Thusly thermal softening is clear in the PMMA. Finite Element simulation of PMMA and PC were conducted using Extended Drucker-Prager Strength (EDP) material model and Hydrodynamic material model with Hugoniots equation of state (Shock EOS Bilinear), respectively.

2.3. Failure criterion for PMMA and PC

To simulate the high strain rate sensitive polymers (PMMA, PC), ANSYS Workbench explicit Dynamic finite element code was used; the geometry is modelled in AUTODESK INVENTOR. For numerical simulation of PMMA and PC, the effects of two failure criteria (ductility and brittleness) were studied with erosion control and element removal. The failure of brittle materials is a tensile failure, which fractures when

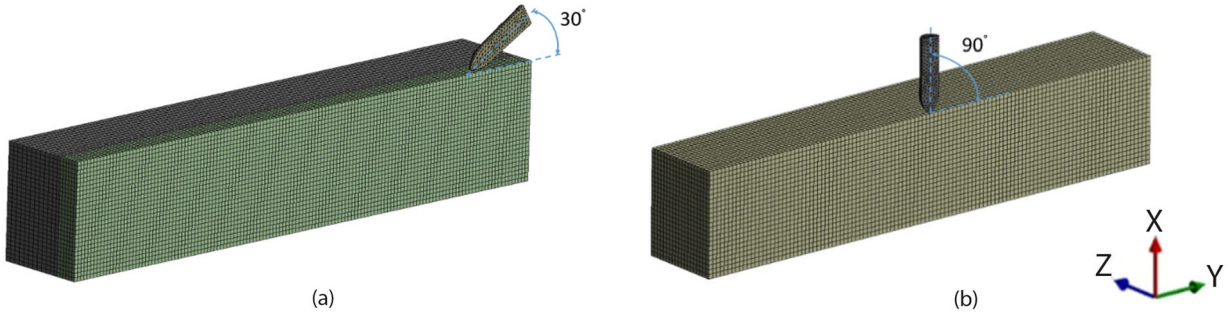

Fig. 2. Projectile impacting plate at 30° (a) and 90° (b).

the tensile stress reaches fracture strength. Damage initiation in ductile failure is due to nucleation and growth of voids in materials where the equivalent plastic strain at the damage initiation is a function of the stress triaxiality η and plastic strain rate $\epsilon^{\cdot}$. Triaxial stress, low temperatures, and high strain rates reduce structural material's ductility locally [15]. Stress triaxiality can affect the rupture by preventing plastic deformation and avoid growing inside the material. This study's failure criterion is a plastic strain, tensile pressure, and significant stress failure with element removal choice. When the failure criterion is met at an element integration point, the material point fails and the element is removed. The failure of ductile materials is a shear failure; according to ductility criterion, the material fails if the maximum shear stress reaches the shear strength, [16]. Stress failure and tensile pressure failure were used to simulate the brittleness. Ductility or plastic strain failure depends on triaxiality, strain rate and temperature; thus, the max equivalent plastic strain criterion is used for simulation.

2.4. Mesh sensitivity analysis

Mesh sensitivity analysis was conducted considering various constant mesh sizes; 1, 1.25, 1.50, 1.75, 2.00 mm, with 352611, 182931, 121849, 76735, 55736 elements, respectively. The mesh convergence was achieved through an iterative method. Fig. 3 illustrates the trajectory of PMMA and PC with various mesh sizes. The projectile has a velocity of 720 $\frac{m}{s}$; its density is 7800 $\frac{Kg}{m^3}$ and the impact angle is 30°. The addition of elements increased the solve time, and the mesh refinement discontinued when the same solution was achieved. The results of stress, deformation, DOP converged to a repeatable solution with decreasing element size. Small red dots in Fig. 3 around the plate show the elements' failure and segmentation. The constant size of the elements throughout the simulation was 1.5 mm and 1.75 mm for PMMA and PC, respectively.

3. Numerical simulation and material model of Polymethyl methacrylate (PMMA)- Plexiglas

The exemplary Drucker Prager criterion is a basic adjustment of the Von-Mises, in that the von Mises standard is changed to incorporate hydrostatic pressure affectability. Albeit the linear Drucker-Prager yield standard incorporates some affectability of yielding to the hydrostatic stress, it cannot describe behaviour with any accuracy under pressure states in which there is a high component of hydrostatic tension. Drucker Prager (DP) is a pressure-dependent material model that can be used to determine whether a material has failed or undergone plastic yielding. Feng et al. [17] have presented strain gradient plasticity theory based on Drucker-Prager (DP) yield function. The Extended Drucker Prager Strength (EDP) material model is used in this study, representing dynamic tensile failure, the spall strength, and characterising yielding to hydrostatic stress [1, 17]. The EDP material model incorporates three yield standards and corresponding flow potentials like those of the exemplary Drucker Prager model utilized for materials with internal cohesion and friction [18]. The yield functions can be combined with anisotropic or kinematic hardening rule to evolve the yield stress during plastic deformation. Eqn. (1) can express rate and pressing factor reliance of the mechanical conduct of PMMA at a high strain rate, as follows:

Table 1. Material properties of PMMA taken from [9].

Density ($\frac{Tonne}{mm^3}$)	ρ	$1.18e^{-9}$
Poisson's Ratio	ν	0.42
Shear Modulus (MPa)	G	2300
Sound Velocity ($\frac{mm}{s}$)	C_0	2.57
Frictional Drucker-Prager angle	β	20°
for ($\dot{\gamma} = 10^2$ to 10^4 $\frac{1}{s}$), to minimize the thermal effects	ϵ	0.06
Pressure sensitivity for high strain rate	α	0.2436
Reference shear flow stress (MPa)	τ_0	124.2
Tensile stress (MPa)	σ	100-150
Yield stress (MPa)	Y	200-350

$$\tau_{flow} = 66.78\dot{\gamma}^{0.06933} + \alpha p \tag{1}$$

Where $\tau_{flow} = 0.5\sigma_{flow}$ is the shear flow stress, α is the pressure sensitivity coefficient, $p = \frac{(\sigma_{flow}+2q)}{3}$ is the hydrostatic pressure, and q is the pressure confinement of the material.

The material is known to have a relatively high dynamic compressive strength of around 250 MPa. This relatively high value of compressive strength results from the high strain rates, which PMMA experiences under dynamic loading condition. The material is also too brittle with a spall strength of $100-150$ MPa [3] and tensile pressure failure of -5 MPa for. This pressure causes plastic deformation within the PMMA plate that corresponds to a high level of Von Mises stress [19]. This failure is accompanied by a maximum equivalent plastic strain (ϵ_P^{max}), pressure sensitivity index (β) and dynamic yield strength. Table 1 shows the material properties used for the FE simulation of PMMA. Numerical analysis performed in this study was compared with the experimental results to validate the simulation's accuracy. Fig. 4 shows the numerical simulation of the PMMA results validated against [3]. It illustrates that the projectile's orientation and position in the target are well imitated with principal stress and tensile pressure failure at the velocity of 720 $\frac{m}{s}$. The representative value of 133 MPa for stress and -5 MPa for tensile pressure failure is used throughout this study to simulate the PMMA. The ration of compressive to spall strength failure is around 20. As the ratio of compression to tension increases, the brittleness of the materials rises. The collapse of the target around the impact area in the simulation is similar to the amount of impairment in numerical and experimental results in [3]. The results show a minimum ductile failure related to the yield stress and the dependency of plastic strain failure on the triaxiality. The material's failure happens through plastic deformation, rupture and cracking. The numerical simulation results illustrated that high compressive strength exerts a large asymmetric force on the projectile during the penetration. This force deflects the projectile's flight line towards the outside, making a "flat U Shaped" POP. This asymmetric force on the projectile will continue to act all through the penetration process. Fig. 5 shows the max stress of PMMA target

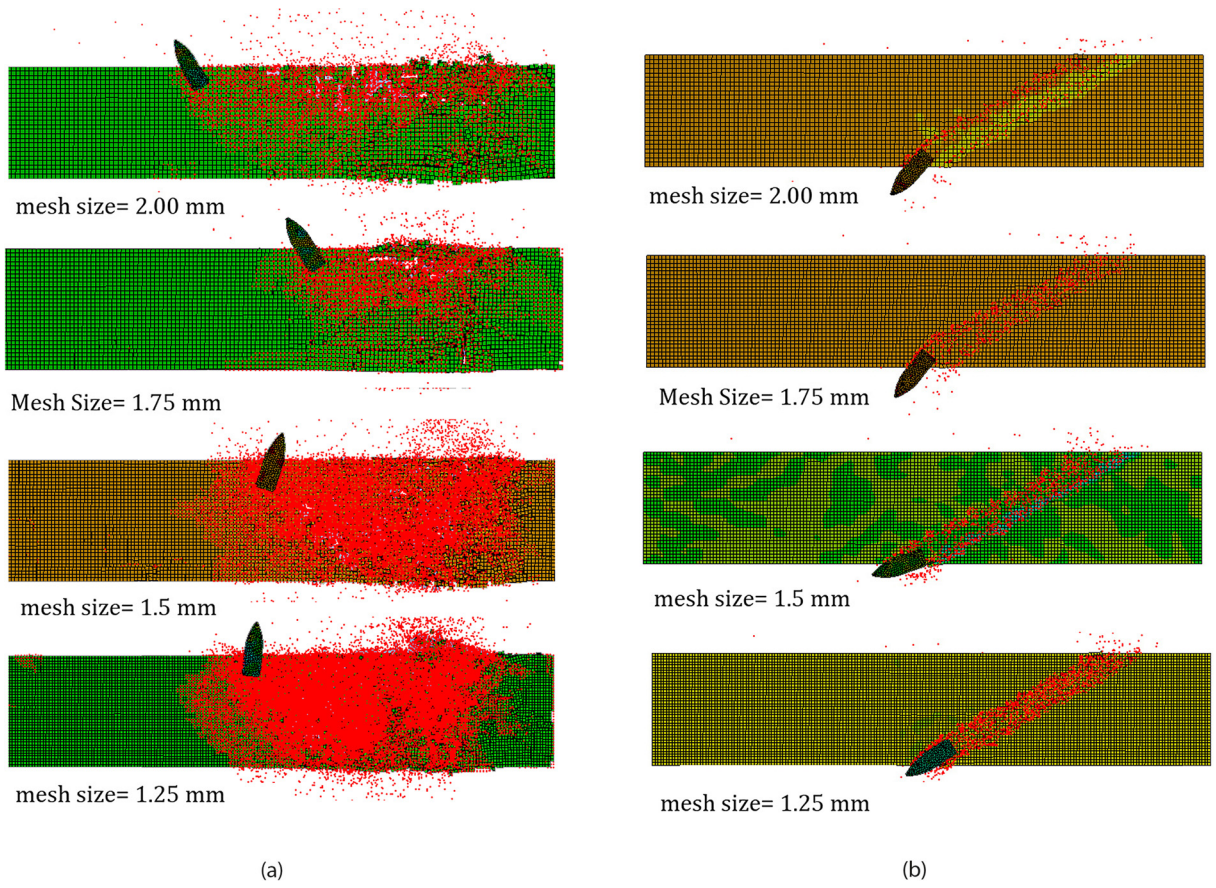

Fig. 3. Comparison between PMMA (a) and PC (b) plate's trajectory with different mesh sizes at 30° and after 200 μs.

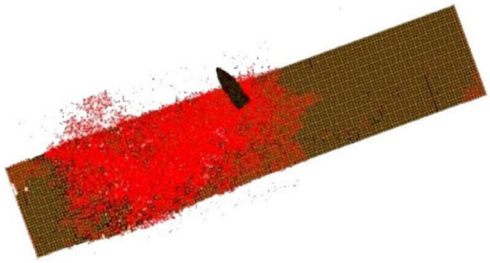

Fig. 4. Trajectory of the projectile at an obliquity of 30°, in a PMMA plate.

at the velocity of 720 $\frac{m}{s}$ at an angle 30°. It shows that the target material near the entrance fails due to release waves from the impacting object and continuously exerts the upward push. As shown in Fig. 5, a large section of the target is shattered, followed by large cracks and segmentation and, finally, the element's removal. The results demonstrated that the material exerts an upward push on the projectile always; therefore, the projectile does not penetrate more deeply due to the tensile failure, which depends on triaxiality.

3.1. The influence of projectile velocity on PMMA target with 30° and 90° impact

Numerical simulation of projectile impacting a PMMA plate were carried out considering five initial velocities for projectile: 720 $\frac{m}{s}$, 600 $\frac{m}{s}$, 500 $\frac{m}{s}$, 400 $\frac{m}{s}$ and 300 $\frac{m}{s}$. The material properties, geometry, failure criteria, mesh and boundary conditions are remained constant as explained in previous section. The effects of different velocities of projectile on PMMA's trajectory, projectile's reflection as well as DOP and POP were analysed. Fig. 6 shows the effects of projectile's initial velocity on PMMA target at an angle of 30°. It demonstrates that the DOP decreases with the decrease of velocity. The absolute path also seems to change as the impact speed increases by comparing the result for 400 $\frac{m}{s}$ to those for the higher speeds. In all the models, the target plate cracked and shattered as the projectile penetrated through it. The POP in all the models illustrates that the projectile deflected from its original impact direction with an asymmetric force that oppositely reflects its flight direction with a "U shaped" path. Fig. 7 illustrates the PMMA plate's trajectory with projectile's impact angle of 90° at different initial velocities "720, 600, 500, 400 and 300 $\frac{m}{s}$" after 120 μs. It shows that the DOP of the projectile decreases as the velocity is reduced from 720 $\frac{m}{s}$ to 600 $\frac{m}{s}$ as well as from 600 $\frac{m}{s}$ to 500 $\frac{m}{s}$ and so on. At 720 $\frac{m}{s}$ PMMA is completely cracked and shattered and the projectile penetrated the target thoroughly. As shown in Fig. 7 at 720 $\frac{m}{s}$ impact velocity the projectile exits the plate before 120 μs but at 300 $\frac{m}{s}$ the material is cracked and ruptured but there is no full penetration. The material near the entrance area is failed with complete perforation, crack propagation and deep penetration as a result of ductile damage and brittleness.

By comparing Fig. 6 and Fig. 7, one can see that there is a significant difference between the DOP and POP at two impact angles 30° and 90°. At the 30° angle, there is a continuous upward push that causes the projectile to deflect from its initial impact direction, whereas it is different at 90° impact. DOP at 90° is much greater than 30° also POP at 90° does not have too much deviation from its initial impact angle.

Fig. 8 shows different impact angle and velocities of the projectile and its effect on Von Mises and intensity stress. The stress is decreasing relatively and linearly as the velocity drops. It illustrates that this stress is relatively high at 720 $\frac{m}{s}$ for both 30° and 90° impact angles, Fig. 8(a) and Fig. 8(b) respectively. The stress is decreasing relatively and linearly as the velocity dropped to 300 $\frac{m}{s}$. The influence of projectile's core density on PMMA target is investigated in Fig. 9(a). It displays

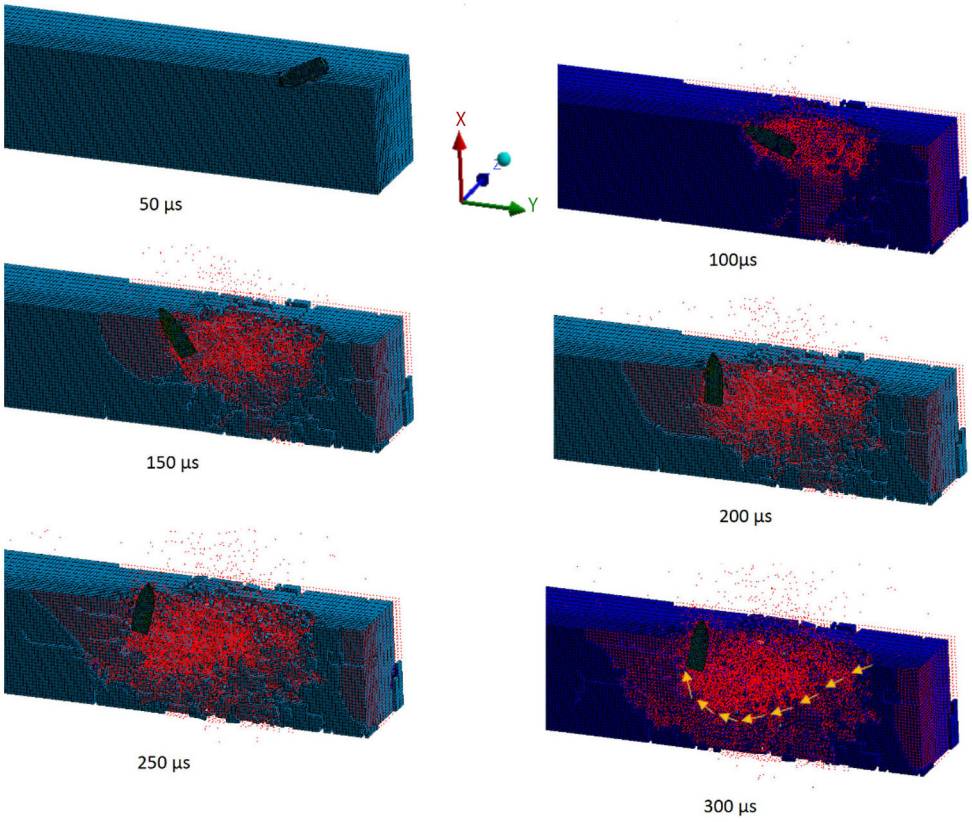

Fig. 5. Time evolution of Maximum principal stress of projectile penetration into brittle PMMA plate at the velocity of 720 $\frac{m}{s}$ and 30°.

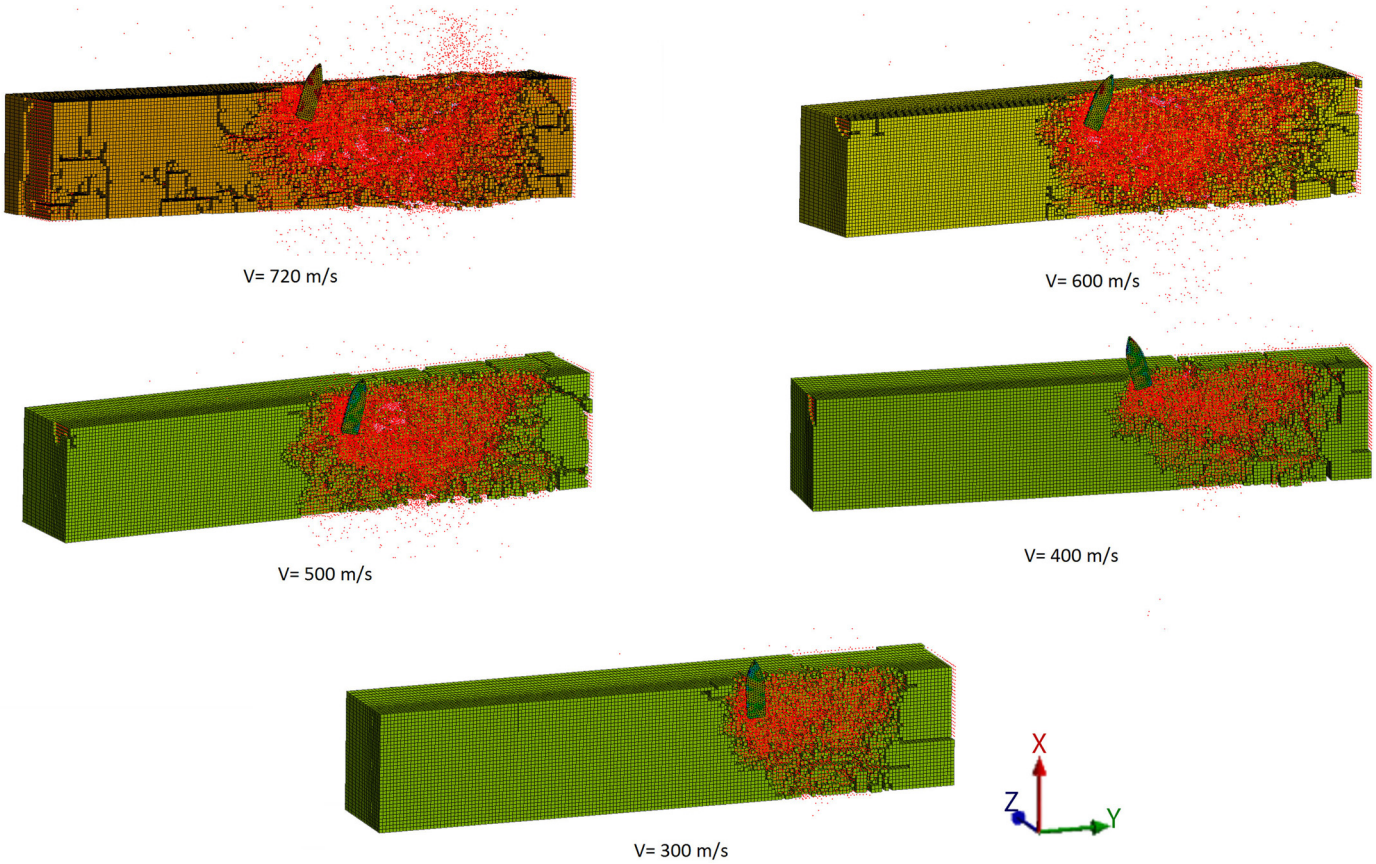

Fig. 6. The influence of projectile's velocity on PMMA plate at an angle of 30° (at 300 µs after impact).

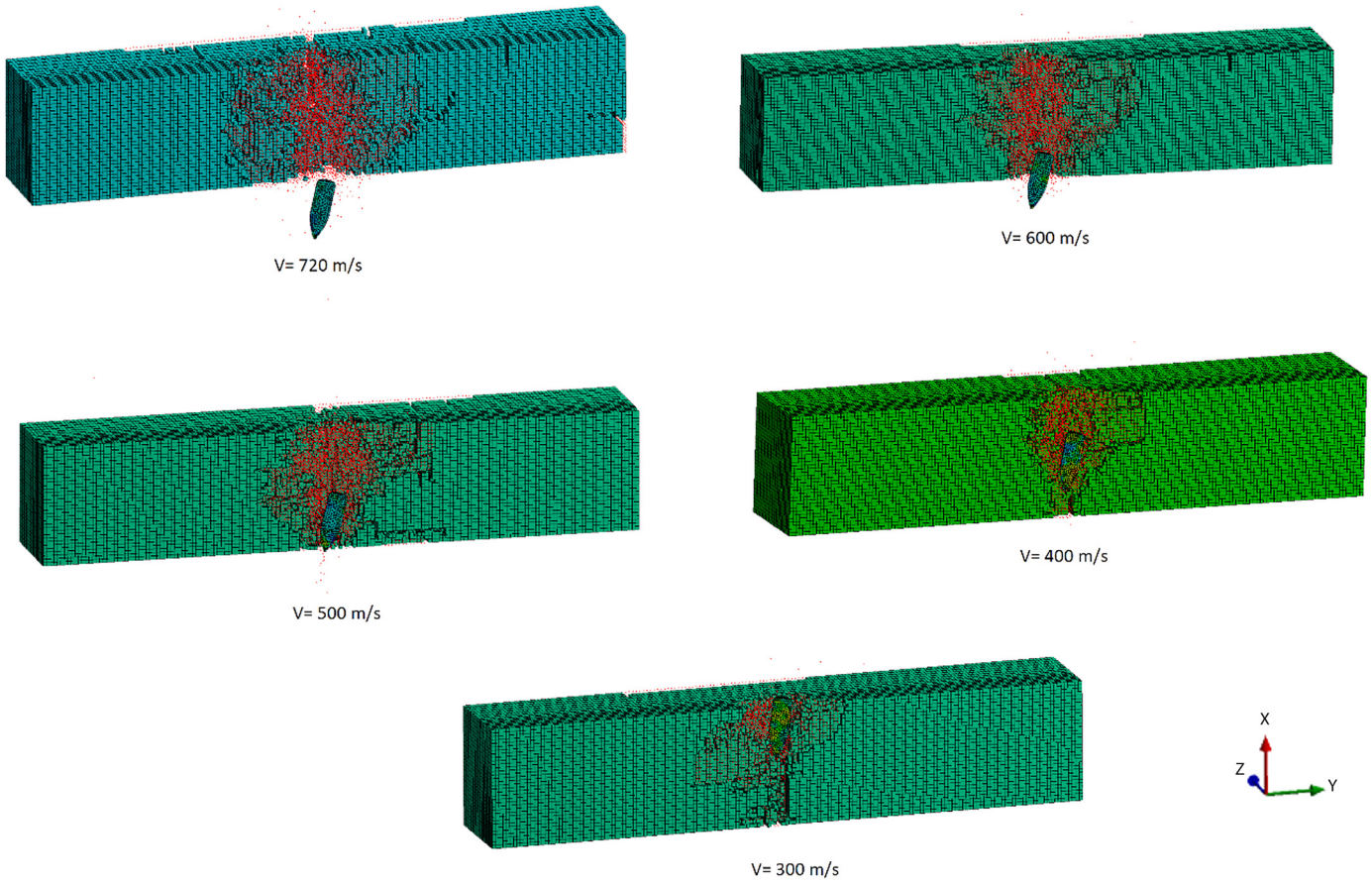

Fig. 7. The influence of projectile's velocity on PMMA plate at an angle of 90° (at 120 μs after impact).

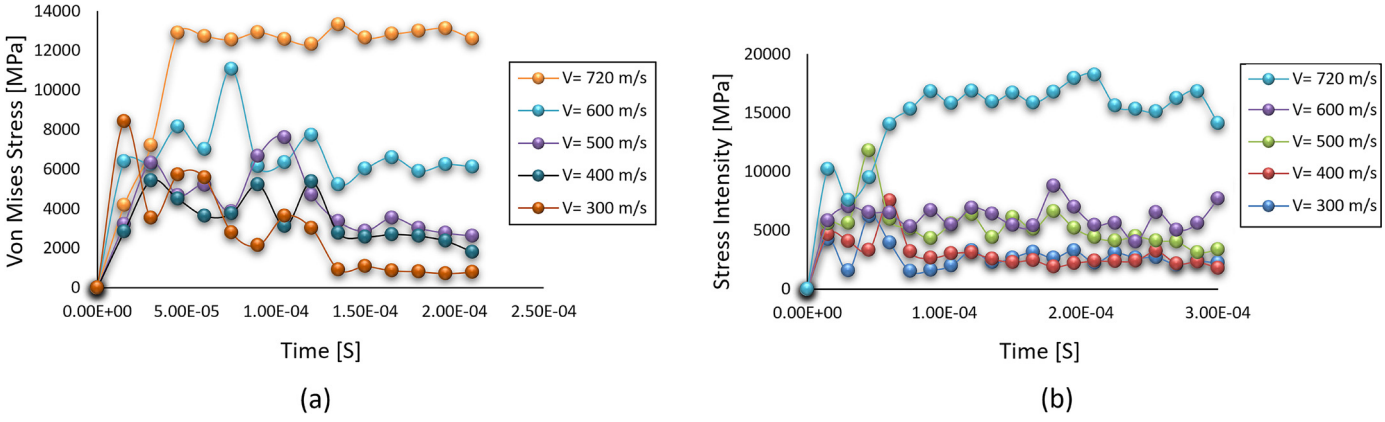

Fig. 8. The effects of projectile's velocity on PMMA's Von Mises stress (a) during the projectile's penetration at an angle of 30° (at 350 μs after impact), and (b) 90° (at 120 μs after impact).

the principal stress of the target at 720 $\frac{m}{s}$ with two different projectile's core density $7.8e^{-9}$ Kg/m^3 and $5.85e^{-9}$ $\frac{Kg}{m^3}$. Projectile with a density of $7.8e^{-9}$ $\frac{Kg}{m^3}$ causes higher stress oscillation which is followed by higher crack and ricochet of the target. Fig. 9(b) demonstrates the projectile displacement along x-axis at various velocities at 30° impact angle. It shows that a push-up follows the displacement along the x-axis, and at 720 $\frac{m}{s}$, the displacement of the projectile has the highest value. At 400 $\frac{m}{s}$ after 200 μs, the projectile starts to move towards the opposite direction. It is different with 300 $\frac{m}{s}$ velocity where the projectile does not have enough kinetic energy to move upwards. The kinetic energy and residual velocity of the projectile changes with different velocities, and this value decreases as the projectile velocity decreases.

Fig. 9(c) shows the projectile's displacement through the target at different velocity at an angle of 90° towards the X and Y-direction. The X-direction displacement is much higher than Y-direction, which means the projectile hovers along this direction rather than following a "U Shaped" path.

4. Numerical simulation and material model of Polycarbonate (PC)- Lexan

Polycarbonate is a polymer with high ductility and yield strain with a significant amount of strain hardening that enables it to display impressive impact and perforation resistance [14]. Under dynamic loading, the deformation and failure of PC occurs at a more little plastic

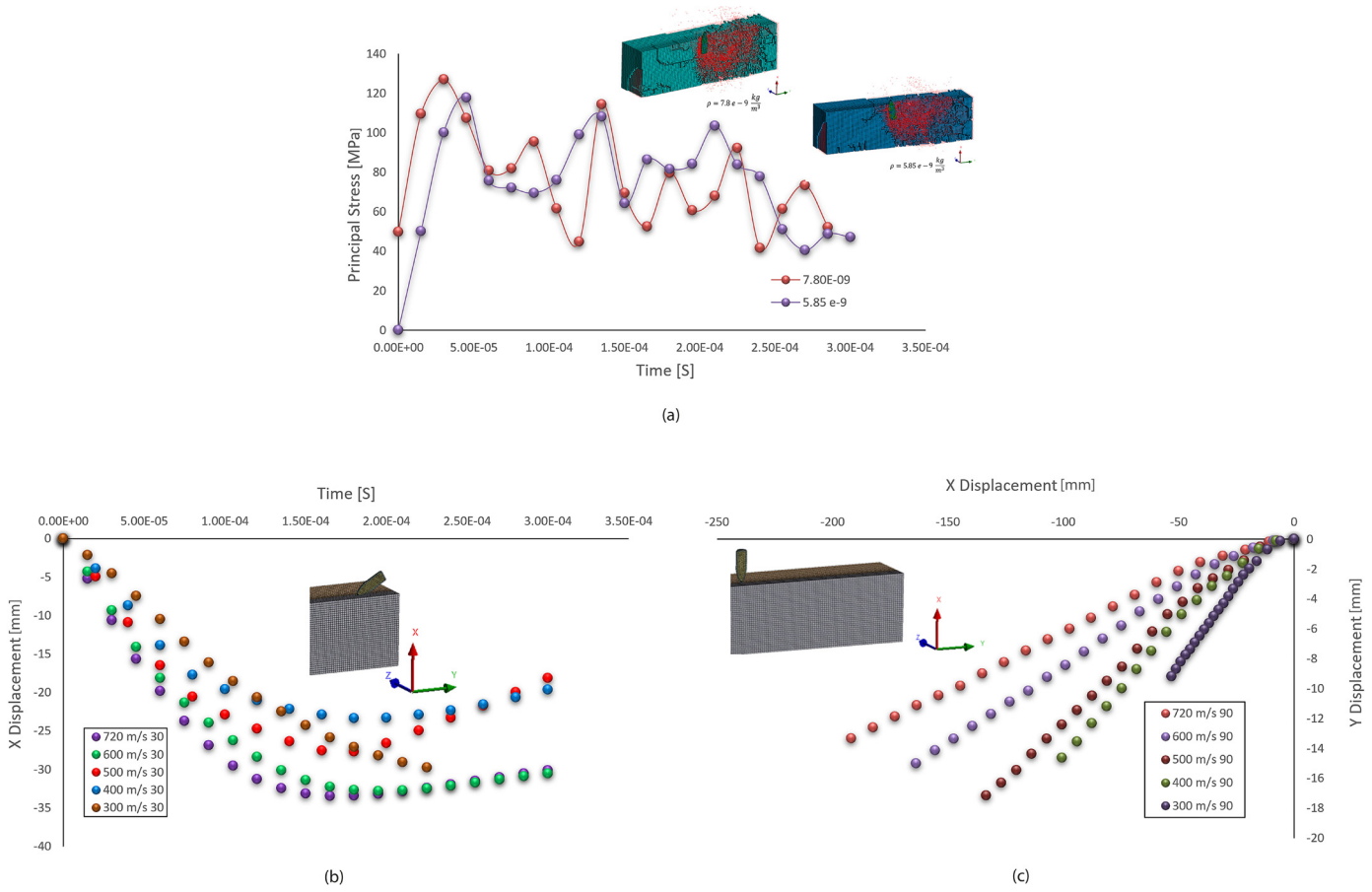

Fig. 9. (a) Effects of projectile's core density on max principle stress at 720 $\frac{m}{s}$. (b) projectile's displacement through target at different velocity of an angle of 30°. (c) projectile's displacement through target at different velocity at an angle of 90°.

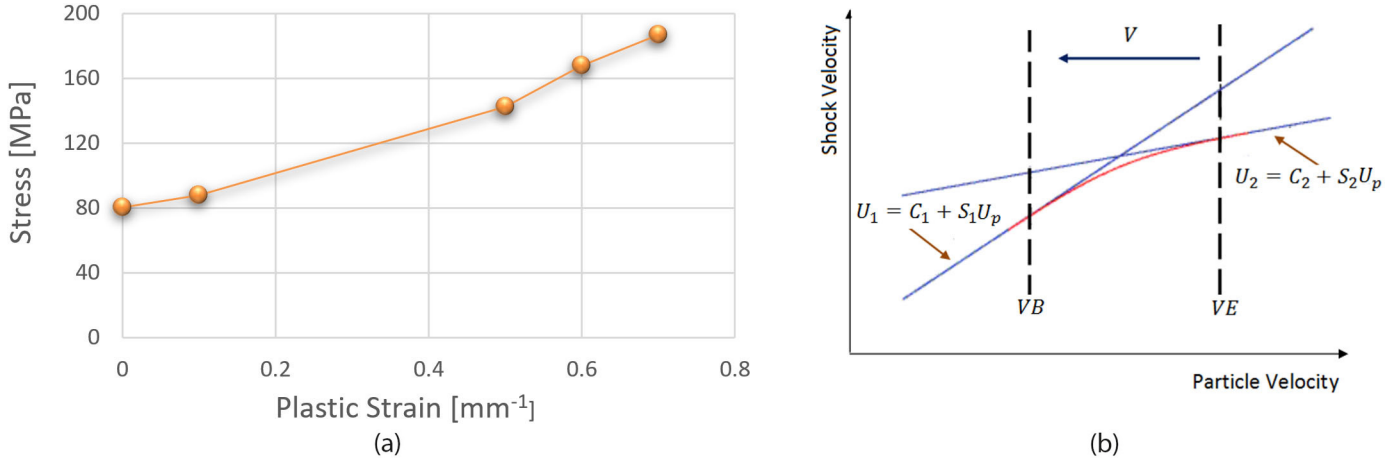

Fig. 10. (a) Multilinear Isotropic Hardening (plastic flow) of PC [20]. (b) Shock Velocity and Particle Velocity Relationship.

strain [21]. Experimental observation of PC plate under ballistic impact shows five deformation mechanism for the plate. These mechanisms are dishing, petalling, deep penetration, cone cracking and plugging [14]. A thin PC plate's ballistic impact displays elastic dishing deformation followed by deep penetration, while thick plates demonstrate deep penetration and yawning penetration. Shock Hugoniots equation of state (Shock EOS Bilinear) is more suitable to simulate materials involving compressible shock flows; thus, it is used to simulate PC where its plastic flow is illustrated in Fig. 10(a). Over an extensive range of shock strengths and nonlinearity, two linear fits to the shock velocity and particle velocity relationship must be approximated by a simple fit as shown in Eqn. (2), [22, 23]:

$$\begin{cases} U_1 = C_1 + S_1 U_P \\ U_2 = C_2 + S_2 U_P \end{cases} \tag{2}$$

U_1 is the shock's speed, U_p is the post-shock particle speed, C_1 is the unshocked medium's speed of sound, and S_1 is related to the unshocked medium's isentropic derivative of the bulk modulus concerning pressure. One at low shock compression defined by $U_P > VB$ and one at high shock compression defined by $U_P < VE$ as illustrated in Fig. 10(b).

Table 2. Bilinear shock EOS Material properties and hydrodynamic data for PC.

Density ($\frac{\text{Tonne}}{\text{mm}^3}$)	ρ	$1.2e^{-9}$
Young's Modulus (MPa)	E	2200
Shear Modulus (MPa)	G	1000
Poisson's Ratio	ν	0.4
Bulk sound Speed ($\frac{\text{mm}}{\text{s}}$)	C_1	$1.933e^6$
Slope	S_1	2.65
Bulk sound Speed ($\frac{\text{mm}}{\text{s}}$)	C_2	$2.35e^6$
Slope	S_2	1.6
Gruneisen Coefficient	Γ	0.61
Compressive yield stress (MPa)	σ	100
Equivalent plastic strain	ϵ	4-6%

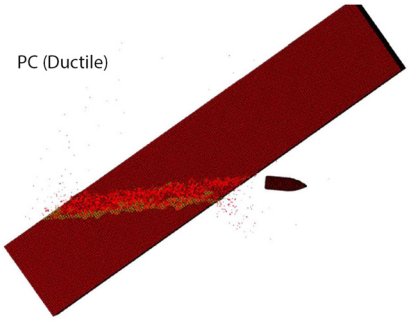

Fig. 11. The PC plate's numerical results and projectile impact velocity of 720 $\frac{\text{m}}{\text{s}}$ at 30°.

$$\begin{cases} U = U_1 & V \le VB \\ U = U_2 & V \ge VE \\ U = U_1 + \frac{(U_2 - U_1)(V - VB)}{(VE - VB)} & VB < V < VE \end{cases} \quad (3)$$

Mechanical property and hydrodynamic material data of PC over a high strain rate $4900 - 8 \times 10^4$ $\frac{1}{\text{s}}$ is provided in Table 2 taken from [14, 22, 24].

PC has higher strain hardening characteristics in tension and compression compared with shear [14]. To validate the numerical simulation in this work, a comparison is performed between numerical simulation and experimental analysis performed by [3, 14]. Fig. 11 shows the plate's penetration (embossing of the projectile in the plate without passing through thoroughly) is followed by "S-shaped" perforation (projectile breaking through the plate). The results illustrate that deep penetration occurs in the target with fragments flow around the projectile. It also shows that the cavity diameter in the entrance and exit is larger than the propagation region. The influence of projectile velocity and density on PC target with 30° and 90° impact. The numerical simulation of projectile and PC target is carried out to investigate each parameter's effects on the PC's trajectory. With a spherical projectile, strains are highest below the bullet's nose, and this highly ductile polymer may demonstrate different failure modes than metals do, [21]. The parameters such as velocity and the projectile's core density are changed one by one while the other factors are considered the same (as explained in the previous section). Five different velocity 720 $\frac{\text{m}}{\text{s}}$, 600 $\frac{\text{m}}{\text{s}}$, 500 $\frac{\text{m}}{\text{s}}$, 400 $\frac{\text{m}}{\text{s}}$ and 300 $\frac{\text{m}}{\text{s}}$ is considered at two different impact angles. The material properties, geometry, failure criteria, mesh and boundary conditions remain constant. The projectile perforates the target when its velocity exceeds the ballistic limit or the mean minimum speed for perforation. Fig. 12(a) plots the projectile's DOP at velocities ranging from 300 to 720 $\frac{\text{m}}{\text{s}}$. It can observe the strong sensitivity of the target's trajectory to the projectile's velocity.

The ductile criterion enforces the projectile follow nearly the straight-line path, whereas the tensile test controls the projectile's way. The penetration of PC targets occurs through the axisymmetric force and in-depth penetration process. The results show that the projectile's lower density can lead to less failure of the goal and, finally, less deflection. According to the results, principal stress and plastic strain failure could simulate brittle and ductile characteristic of PMMA and PC plates and yield an acceptable reproduction of experimental results. The PC target with various velocities at normal impact is plotted in Fig. 12(b). It shows the ballistic limit velocity of the plate that is the critical impact velocity corresponding to a 50% probability of success in defeating the target ($v < v_{50}$). The projectile penetrates and perforates the plate in all the simulated models with different residual velocities relative to its initial velocity. The region around the penetrating projectile undergoes shear yielding as, and PC target changes the reflective index as it yields [14].

The numerical and experimental path of the PC plate at 750 $\frac{\text{m}}{\text{s}}$ is depicted in Fig. 13 that is taken from [25] and compared with numerical results in this work. The numerical data are smoothed and show projectile's movement towards (x, y) direction with three reigns of the trajectory known as a. entrance, b. propagation, and c. exit. A good agreement can be observed for the main characteristics of the trajectory. With all the velocities, the projectile fully penetrated the target, but the penetration takes a longer time to happen as the velocity decreases. This parameter also has significant effects on the DOP since as the velocity decreases, DOP drops. The influence of the projectile's impact angle can be demonstrated through the time progress of elastic strain at 720 $\frac{\text{m}}{\text{s}}$ as shows in Fig. 14. It shows the evolution of projectile deflection and it's penetration at the target. It displays that with 90° impact, POP is "J shape", which is different from 30° which is "S shape". The deflection, which is the angle between the projectile's initial direction and its way out, is small. The results showed that with an impact angle of 90°, the projectile perforates and exits the target with an orientation nearly parallel to the initial impact angle. The effects of different velocity with 90° impact angle are displayed in Fig. 14. It shows the impact of this factor on penetration depth (DOP) and indicates that DOP scales linearly with the impact velocity. The results also display the deep penetration, and plugging is the failure process of the thick PC.

5. Conclusion and discussion

A comprehensive study of the dynamic failure of monolithic PC and PMMA targets are studied at various impact velocities and projectile's core density with the inclined and normal impact of 30° and 90°. Only half the models were simulated due to the symmetrical nature of the simulated models [3]. The results showed that these two materials could deflect the projectile's course of the flight from its initial angle of penetration. During projectile penetration at 720 $\frac{\text{m}}{\text{s}}$ and the oblique impact on PC, projectile follows an "S-shaped" passage with 30° impact, and the maximum stress was 2.29 GPa, whereas PMMA showed a "flat U shaped" POP with a small DOP and maximum stress of 5.16 GPa. PMMA target was entirely shattered and failed, confirming the brittle-ductile characteristic of the material with the residual velocity of 293.8 $\frac{\text{m}}{\text{s}}$. The residual velocity of the PC was 244 $\frac{\text{m}}{\text{s}}$.

The results showed that the Extended Drucker Prager Strength (EDP) material model with the failure criteria's of principal stress and tensile pressure failure could simulate the PMMA characteristics. It also has been found that these two materials exert a strong asymmetric force on impacting projectile, which results in its strong deflection.

Shock Hugoniots equation of state with plastic strain failure is successfully simulated the specific characteristic of PC target. The results showed that the Extended Drucker Prager Strength (EDP) material model with the failure criteria's of principal stress and tensile pressure failure could simulate the PMMA characteristics. It also has been found that these two materials exert a strong asymmetric force on impacting projectile, which results in its sharp deflection. Shock Hugoniots equation of state with plastic strain failure is successfully simulated the specific characteristic of PC target. The results showed the importance of material properties and their failure criteria, which manages these polymers' brittleness and ductility. The projectile's DOP and POP are affected by the initial impact velocity, the density of the projectile's

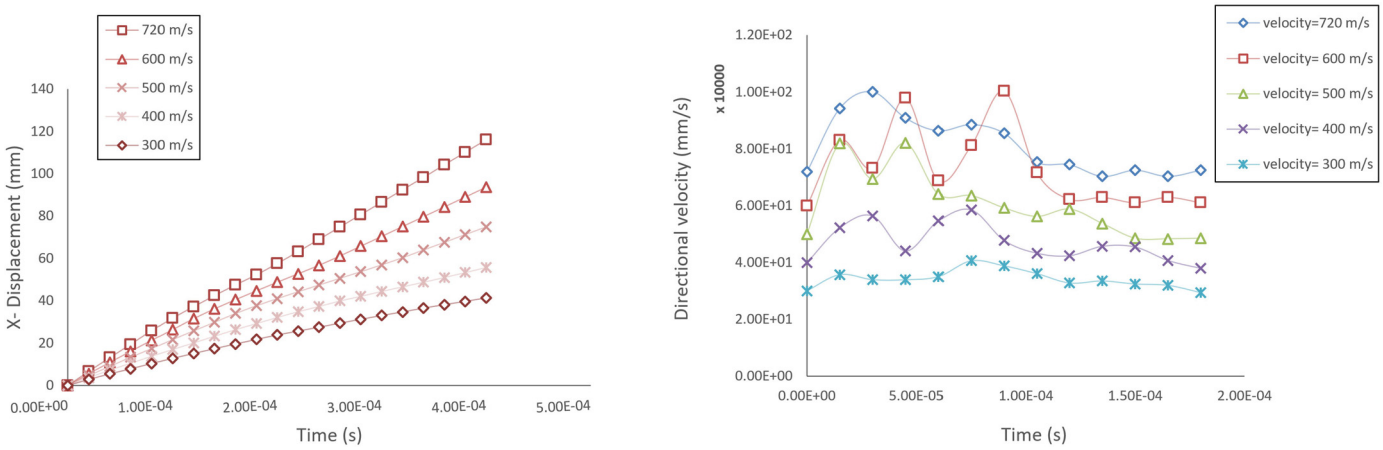

Fig. 12. (a) Projectile's DOP at various velocity and an angle of 30°. (b) The directional velocity of the projectile after impacting PC target at 90°.

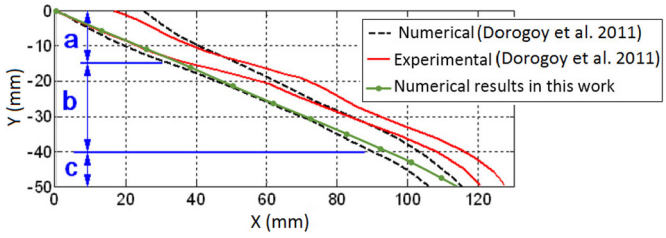

Fig. 13. Comparison between numerical and experimental trajectory of target at 30°.

core projectile, kinetic energy, and the plates. It is also demonstrated that DOP scales linearly with the impact velocity. The results confirmed that PMMA, like other brittle materials, falls into the pressure-induced brittle-ductile transition materials category [25], which indicates that the material strength of PMMA grows with the increase of pressure sensitivity index (β). The projectile's penetration into the target deflects from its original impact axis and stops with an active drag force proportional to its initial velocity value.

Future research will study the possibility of creating a model that can accurately predict the output results of FE analyses of PC and PMMA to describe the behaviour of materials under various loading conditions. The predictive models will be created through Artificial Neural Networks (ANNs) for design optimisation.

Declarations

Author contribution statement

Shabnam Sadeghi Esfahlani: Conceived and designed the experiments; Performed the experiments; Analyzed and interpreted the data; Contributed reagents, materials, analysis tools or data; Wrote the paper.

Declaration of interests statement

The authors declare no conflict of interest.

Data availability statement

Data included in article/supp. material/referenced in article.

Funding statement

This work was supported by the Low Carbon KEEP programme 'European Regional Development Fund (ERDF) - East of England Development Agency' and Essex Safety Glass (ESG).

Additional information

No additional information is available for this paper.

References

[1] P. Bardia, R. Narasimhan, Characterisation of pressure-sensitive yielding in polymers, Strain 42 (3) (2006) 187–196.
[2] S. Sarva, A.D. Mulliken, M.C. Boyce, A.J. Hsieh, Mechanics of transparent polymeric material assemblies under projectile impact: simulations and experiments, in: Transformational Science and Technology for the Current and Future Force: (with CD-ROM), World Scientific, 2006, pp. 227–234.
[3] Z. Rosenberg, Z. Surujon, Y. Yeshurun, Y. Ashuach, E. Dekel, Ricochet of 0.3 ap projectile from inclined polymeric plates, Int. J. Impact Eng. 31 (3) (2005) 221–233.
[4] J. Richeton, S. Ahzi, K. Vecchio, F. Jiang, A. Makradi, Modeling and validation of the large deformation inelastic response of amorphous polymers over a wide range of temperatures and strain rates, Int. J. Solids Struct. 44 (24) (2007) 7938–7954.
[5] A. Varghese, R. Batra, Constitutive equations for thermomechanical deformations of glassy polymers, Int. J. Solids Struct. 46 (22–23) (2009) 4079–4094.
[6] A. Mulliken, M. Boyce, Mechanics of the rate-dependent elastic–plastic deformation of glassy polymers from low to high strain rates, Int. J. Solids Struct. 43 (5) (2006) 1331–1356.
[7] J. Richeton, S. Ahzi, K. Vecchio, F. Jiang, R. Adharapurapu, Influence of temperature and strain rate on the mechanical behavior of three amorphous polymers: characterization and modeling of the compressive yield stress, Int. J. Solids Struct. 43 (7–8) (2006) 2318–2335.
[8] S. Satapathy, S. Bless, Deep punching pmma, Exp. Mech. 40 (1) (2000) 31–37.
[9] D. Rittel, A. Brill, Dynamic flow and failure of confined polymethylmethacrylate, J. Mech. Phys. Solids 56 (4) (2008) 1401–1416.
[10] F. Chen, Y. Peng, X. Chen, K. Wang, Z. Liu, C. Chen, Investigation of the ballistic performance of gfrp laminate under 150 m/s high-velocity impact: simulation and experiment, Polymers 13 (4) (2021) 604.
[11] C. Zhang, Q. Zhu, J.L. Curiel-Sosa, T.Q. Bui, Ballistic performance and damage simulation of fiber metal laminates under high-velocity oblique impact, Int. J. Damage Mech. 29 (7) (2020) 1011–1034.
[12] Y. Chen, B. Pang, W. Zheng, K. Peng, Experimental investigation on normal and oblique ballistic impact behavior of fiber metal laminates, J. Reinf. Plast. Compos. 32 (23) (2013) 1769–1778.
[13] Q. Li, E. Flores-Johnson, Hard projectile penetration and trajectory stability, Int. J. Impact Eng. 38 (10) (2011) 815–823.
[14] S. Wright, N. Fleck, W. Stronge, Ballistic impact of polycarbonate-an experimental investigation, Int. J. Impact Eng. 13 (1) (1993) 1–20.
[15] G. Maresca, P. Milella, G. Pino, A critical review of triaxiality based failure criteria, in: Proc Convegno IGF13 Cassino, 1997.
[16] A.-H. Lee, Finite element simulations with ANSYS workbench 15: theory, applications, case studies, https://books.google.co.uk/books?id=Zh3GNd9M1oUC&printsec=frontcover&source=gbs_ge_summary_r&cad=0, 2014.
[17] L. Feng, Y. Kang, G. Zhang, S. Wang, Mechanism-based strain gradient Drucker–Prager elastoplasticity for pressure-sensitive materials, Int. J. Solids Struct. 47 (20) (2010) 2693–2705.
[18] A. Guide, ANSYS advanced analysis techniques guide, http://imechanica.org/files/AdvacedAnsys.pdf, 2005.
[19] D. Rittel, A. Dorogoy, Impact of thick pmma plates by long projectiles at low velocities. Part I: effect of head's shape, Mech. Mater. 70 (2014) 41–52.
[20] P.J. Hazell, C.J. Roberson, M. Moutinho, The design of mosaic armour: the influence of tile size on ballistic performance, Mater. Des. 29 (8) (2008) 1497–1503.

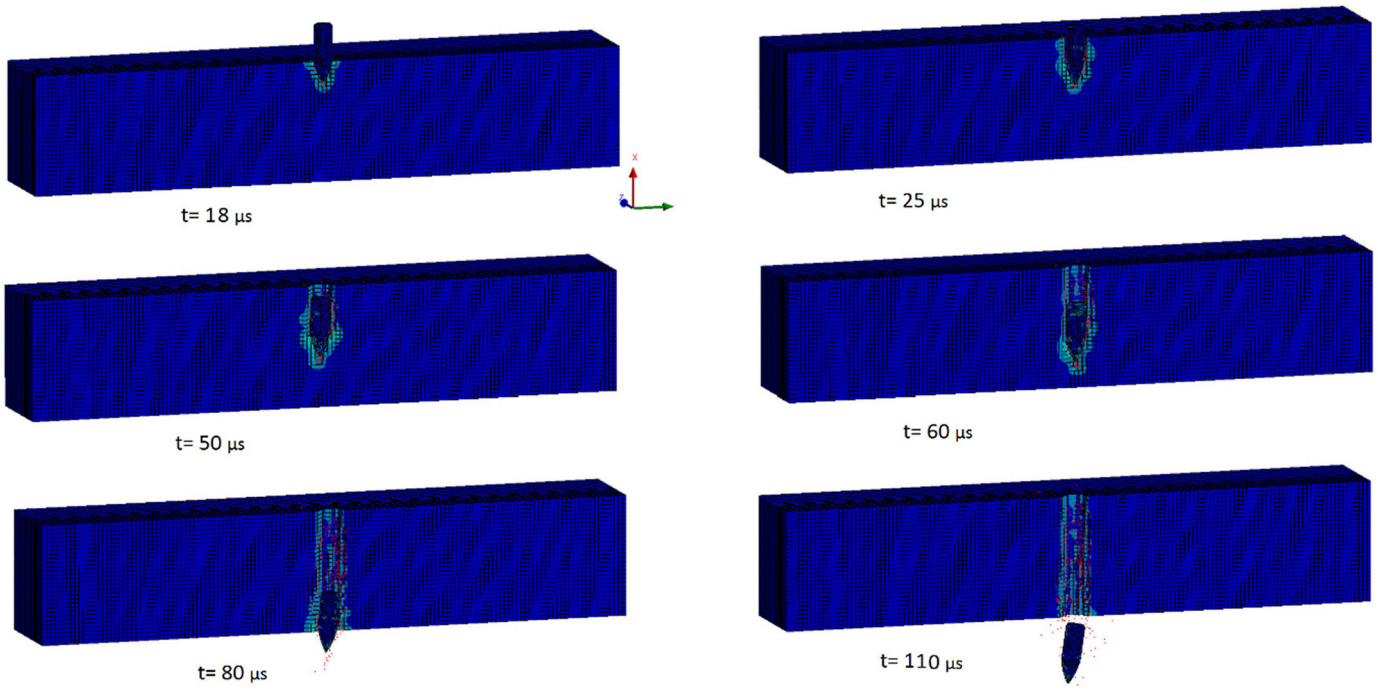

Fig. 14. Time evolution of Elastic strain of PC plate at the velocity of 720 $\frac{m}{s}$ and 90° impact of the projectile.

[21] Q.H. Shah, Impact resistance of a rectangular polycarbonate armor plate subjected to single and multiple impacts, Int. J. Impact Eng. 36 (9) (2009) 1128–1135.
[22] J. Millett, N. Bourne, Shock and release of polycarbonate under one-dimensional strain, J. Mater. Sci. 41 (6) (2006) 1683–1690.
[23] G.M. Ward, The simulation of shock- and impact-driven flows with Mie-Grüneisen equations of state, Ph.D. thesis, California Institute of Technology, 2011.
[24] P. Hazell, M. Edwards, H. Longstaff, J. Erskine, Penetration of a glass-faced transparent elastomeric resin by a lead–antimony-cored bullet, Int. J. Impact Eng. 36 (1) (2009) 147–153.
[25] A. Dorogoy, D. Rittel, A. Brill, Experimentation and modeling of inclined ballistic impact in thick polycarbonate plates, Int. J. Impact Eng. 38 (10) (2011) 804–814.